Chemical routes to materials

Enhancement of the low-temperature catalytic graphitization of polyacrylonitrile by incorporating Cu nanostructures as plasmonic photocatalyst

Zhengdong Zhang[1], Jianchen Lu[1], Xiang Ren[1], Nan Sun[1], Jianqi Liu[1], Yan Zhou[1], Yu Gao[1], Jinming Cai[1], Xiaoming Cai[1], and Honglin Tan[1,*] (ORCID)

[1] Faculty of Materials Science and Engineering, Kunming University of Science and Technology, Kunming 650093, Yunnan, People's Republic of China

ABSTRACT

Here, we systematically investigate the chemical process of low-temperature catalytic graphitization of polyacrylonitrile (PAN) by using roughened copper (Cu) nanostructures as a plasmonic photocatalyst. Our in situ surface-enhanced Raman scattering spectroscopy (SERS) results show that the PAN coated on the Cu surface is successfully converted to graphite at 120 °C. The gradual increase of radiation power in the SERS leads to a significant reduction of the number of defects formed in the graphite, which will not be caused by employing longer duration laser. Moreover, when the average size of the copper nanostructures is about 40 nm, the PAN has the largest graphitization degree. In order to simulate the impact of the different Cu nanostructure sizes on the local electric field distribution, we performed a self-consistent numerical model calculation (finite-difference time-domain, FDTD). The calculated results show that the local electric field distribution presents a strong dependence on the size of the Cu-based nanostructures. The experimental results are in direct line with the assumption that the excitation on plasmonic nanostructures results in increased generation rates of hot carriers due to the local electric field enhancement.

Introduction

It is well established that polyacrylonitrile (PAN)-based carbon materials are considered to be excellent candidates for reinforcing applications due to their excellent mechanical properties as well as their promising chemical stability [1]. Over the past few decades, great efforts have been carried out to increase the degree of carbon graphitization toward improving their electrical, thermal, and mechanical properties. In general, the graphitization temperature of PAN-based carbon fibers can be as high as 2400 °C

Handling Editor: Pedro Camargo.

Address correspondence to E-mail: 852419171@qq.com

[2]. The conventional techniques that solely rely on heating procedures to increase the degree of graphitization consume a high amount of power that inevitably leads to higher manufacturing costs. In addition, the catalytic graphitization properties of carbon materials have been also investigated by employing various doping procedures, such as using various refractory-metal carbides, including WC, TiC, VC, and ZrC, as well as elements like Ti, Zr, B, and Si [3, 4]. However, there are few reports in the literature that plasmonic photocatalysis system can enhance the catalytic graphitization performance of PAN molecules by plasmon-induced hot-carrier generation effect. This challenge can be addressed by leveraging the surface plasmon resonance (SPR) effect that takes place on the surface of metal nanostructures. Until now, surface-enhanced Raman scattering (SERS) spectroscopy, which is also based on the SPR effect, has been widely applied to initiate the respective photochemical reactions [5–7]. Along these lines, we can use this technique to investigate the low-temperature catalytic graphitization performance of PAN molecules.

SPR effect relies on the interaction between free electrons on metallic surfaces and the applied electromagnetic fields [8, 9]. The excitation of surface plasmons (SP) leads to the generation of hot charge carriers [10] that can initiate chemical reactions [5, 11], whereas the induced local heating [12] can also accelerate the rate of the respective surface reactions [13–15]. The relative high energy of the generated hot carriers can be also employed to overcome the potential barrier of chemical reactions, which permit the excitation of molecules under mild interaction conditions, in terms of local heat distribution, and induce chemical reactions that are energetically unfavorable under standard conditions [16, 17].

Normally, light-driven chemical processes on plasmonic nanostructures rely primarily on the employment of conventional Ag and Au substrates [18, 19]. However, the high cost and scarcity of these noble metals have limited their practical application as active photocatalyst elements. In contrast, Cu is widely abundant on Earth and exhibits also outstanding plasmonic properties [20]. Therefore, Cu may be also a promising candidate for the realization of plasmon-induced photocatalytic effects [21]. Moreover, the employment of Cu-based nanostructures as plasmonic photocatalysts for the improvement of catalytic graphitization properties of PAN has not been yet thoroughly investigated.

In this work, we report the fabrication of Cu-based metallic surfaces with high surface roughness for enhanced SPR effect, and we examine the impact of various experimental parameters, including the radiated power of SERS, the radiation time and the size of the Cu-based nanoparticles on the PAN graphitization processes, by using in situ SERS spectroscopy. In addition, we elucidate on the origins of the potential mechanism for enhancing the catalytic graphitization properties of PAN, by employing the FDTD method in order to account for the influence of the different Cu nanostructure sizes on the local electric field distribution. Our theoretical approach reveals good consistency with the respective experimental data, denoting the validity of our model.

Experimental section

Preparation of the roughen Cu surfaces

A Cu substrate with outstanding plasmonic optical properties was used as the active SERS substrate. The Cu foil is placed in acetone solution for ultrasonic cleaning for 20 min and then cleaned with ethanol and distilled water to ensure the cleanness of the copper foil. To ensure the necessary SERS activation, a roughening procedure was implemented on the copper substrates. We used a nitric acid solution with a concentration of 2.5 M to etch the smooth copper surface for 10, 20 and 30 min, respectively (see Supplementary Information Figure S1). Their sizes are 25 nm, 40 nm, and 80 nm, respectively, obtained by using AFM to characterize surface of Cu foil.

Raman and SERS measurements

The PAN reactant was used for SERS detection and the SP-induced reduction reaction. Initially, the PAN reactant was dissolved in a solvent from dimethylformamide (DMF) in order to obtain a solution with a 2% concentration. The PAN was uniformly spin-coated on Cu foil and Si/SiO$_2$, respectively, by using a spin-coater. SERS spectra were collected using a Renishaw inVia Raman microscope under 532 nm laser excitation. In SERS studies, to confirm that catalytic graphitization of PAN is triggered by hot

carriers generated in the Cu nanoparticles, different laser powers were used for measurements: 1 mW, 2.5 mW, 5 mW, 12.5 mW, 25 mW, 50 mW. The excitation wavelength was 532 nm where the exposure time is 15 s.

Characterization

The morphology of the samples was characterized by atomic force microscopy (AFM). XPS (Ultra DLD Kratos Axis) instrument was used to identify the binding energies as well as the chemical states of Cu surface.

Finite-difference time-domain (FDTD) simulations

Electrodynamics simulations were carried out using the FDTD method in order to study the optical characteristics of the Cu structure. The choice of model structure depended mainly on the AFM image of the copper nanostructure. All AFM images were inputted to an *FDTD* software to obtain Model 1, Model 2 and Model 3. (see Supplementary Information Figure S2) Cu is illuminated at the plane wave (532 nm) with normal incidence along *Z*-axis and polarization along *X*-axis. *X*-, *Y*- and *Z*-axis direction was bounded by the perfectly matched layers (PML) with 96 nm thickness in order to absorb the scattered light from NSs and suppress the back-scattered light from the outer boundary of the calculated region. For the mesh selection, a grid of 5 nm along *x*, *y*, and *z* directions was chosen. The frequency-dependent complex permittivities of Cu and CuO were obtained from the literature [22, 23]. The frequency-dependent complex permittivities of Cu and CuO are shown in Figure S3 in the supporting information.

Results and discussion

Photocatalysis and in situ SERS study simultaneously

PAN is a straight-chain chemical compound that is formed by the free radical polymerization of the respective monomer acrylonitrile molecule. The molecular chains of PAN are attached with a cyano group. Figure 1A illustrates the chemical structural formula, the ball-and-stick model and the macroscopic representation of PAN. The material is finally formed under powder configuration and exhibits white color. In order to carry out the SERS experiment, we employed Cu substrate with outstanding plasmonic optical properties. Moreover, in order to secure the necessary conditions for the manifestation of the SERS effect, a roughening procedure was implemented on the copper substrates, resulting in nanoscale surface structures, as evidenced by microscopic investigation (Fig. 1B(a, b)). The desired surface roughness was acquired after etching in nitric acid solution the smooth copper substrate, as it is depicted in Fig. 1B(b). Within these modified nanoscale structures, the excitation of electrons from the metal surface can be confined by employing an external light field in order to induce the plasmon resonance effect [24].

As far as the deposition methods are concerned, the spin-coating technique was used since it produces thin films with a high degree of quality and good uniformity. As it is divulged in Fig. 1B(c), PAN was uniformly spin-coated on the roughed Cu surface and subsequently was subjected to thermal annealing treatment. The employment of the annealing treatment step within our experimental process is necessary in order to remove from the deposited film the volatile solvent. Thus, we retained the annealing temperature constant at 120 °C. More importantly, the PAN molecules are better able to adsorb to the copper surface. Subsequently, we use SERS to explore the interactions between adsorbed chemical species (PAN) and plasmonic catalysts. Figure 1(C) discloses both the Raman spectra of PAN on Si/SiO$_2$ substrate (Red line) as well as the in situ SERS spectra of PAN molecules converted to graphite on Cu foil (Black line). We can clearly see that without a copper substrate, it is impossible to obtain graphite from PAN on Si/SiO$_2$. Fig. S3 shows that the positions of Raman peaks of PAN powder and PAN on Si/SiO$_2$ substrate are consistent (see Supplementary Information Figure S4). Raman peaks of the PAN molecules are mainly located at the following wavenumbers: 1470 cm^{-1} (δ-CH), 2240 cm^{-1} (υ-C≡N), and 2930 cm^{-1} (υ-CH$_2$). From the analysis of SERS peaks of the catalytic reactions where PAN molecules are involved, it is apparent that the structure of PAN has been changed. The complete disappearance of characteristic nitrile group (–C≡N) of PAN, more importantly, the G and D peaks of the graphite appear in the SERS spectra. Moreover, the peaks at
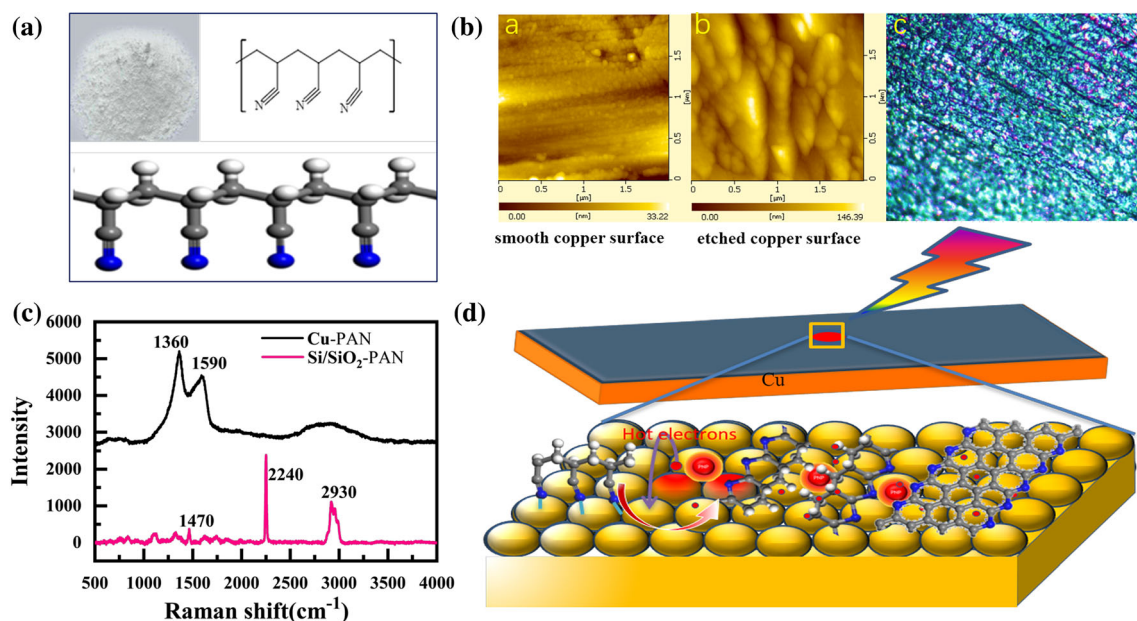
Figure 1 Schematic representation of the photocatalysis and the in situ SERS characterization. **A** The chemical structures and macroscopic appearance of PAN molecules. **B** AFM images of a smooth copper surface (a) and an etched copper surface (b). Optical image of PAN molecules on rough Cu surface after the thermal annealing process (c). **C** SERS spectra of the transformation of PAN molecules to multi-layer graphite on Cu foil. **D** The proposed mechanism of PAN conversion to multi-layer graphite by plasmon-induced hot carriers.

1590 and 1360 cm^{-1} correspond to the G band related to the vibration of sp2-bonded carbon atoms and the D band associated with the vibrations of carbon atoms having dangling bonds in plane terminations of disordered graphite. The Peak G corresponds to the E_{2g} vibration mode of graphite-like crystallites, which represents the amount of ordered structures in graphite-like materials; The Peak D corresponding to the A_{1g} vibration mode of graphite planes indicates the amount of crystal boundaries, disorderly arranged and low symmetry structures in graphite [25]. The position and shape of the G peak confirm also the formation of the sp^2 carbon orbital and provide further pieces of evidence for the presence of the graphite layer [26].

Furthermore, from the Raman spectrum analysis, it is concluded that the PAN molecules are adsorbed on the Cu surface, which was transformed into graphite under the irradiation of 532 nm wavelength. This could be attributed to the ability of plasmonic nanostructures to efficiently collect the energy of a photon beam to a minimal volume at their surface and subsequently transfer this energy to the adsorbed molecules through the activation of electrons, driving thus the photochemical conversion of PAN on Cu-based nanostructures. From our experimental results,

where the catalytic graphitization procedures of PAN molecules on roughed copper surfaces using in situ SERS were thoroughly investigated, a possible reaction mechanism is presented in Fig. 1D. Since both the SERS effect and the hot-carrier generation process originate from the plasma decay process, we speculate that the induced hot carriers can support the chemical reactions of PAN molecules when they are tightly adsorbed on the rough copper surface. In addition, some research work has reported that decay of plasmon generates hot carriers through interband transitions and intraband transitions [27, 28]. To better understand the two types of electronic excitation, the energy band structure and the density of states (DOS) of the copper were calculated by the density functional theory (DFT) method (see Supplementary Information Figure S5).

Impact of hot-carrier generation yield on the catalytic graphitization properties of PAN molecules

In the previous section, we provide some preliminary data regarding the catalytic graphitization properties of PAN molecules that are closely connected with hot-carrier generation procedures within the Cu-

based nanostructures. In order to confirm this assumption, we investigated the photochemical conversion properties of PAN molecules by carrying out various laser irradiation experiments with different power. Along these lines, the catalytic conversion of the PAN molecules to the graphite layer on the Cu foil cannot be achieved by using laser irradiation (a Raman spectroscopy light source) with a total power of 1 mW. The respective D and G peaks of the graphite film appear by employing laser irradiation power of 2.5 mW. In addition, the relative intensity of the D and G peaks gradually increases by enforcing laser with higher power (Fig. 2(A)). From these results, it is clearly demonstrated that the catalytic graphitization reaction is mainly activated by the presence of light. In addition, the ratio of the D and G peaks (I_D/I_G) is frequently used as a method in order to characterize the density of defects within the graphite structure. By enhancing the laser power, the intensity of the G peak increases and subsequently the ratio between the D and G peaks gradually decreases, indicating that the degree of the graphitization process is strengthened (Fig. 2(B)). This effect suggests that the graphitization reaction exhibits a linear relationship from the applied laser power, which is a typical signature of hot-carrier-driven chemical reactions [5, 29]. Thus, the interaction of a high-intensity laser with a roughed Cu foil leads to the formation of energetic charge carriers. The energy transfer from these carriers to the PAN adsorbates could interpret the electron-induced surface reactions and the further reduction of the graphite defects.

Macroscopically, SPR is the result of the interaction of plasma particles with the resonant frequency of light, which converts light energy into heat, and the heat generated is confined to the surface of the metal nanoparticles [30]. So, we have also investigated the influence of plasmon heating on this reaction. In the catalytic reaction, heating is usually used to improve the energy of molecular thermal movement and realize molecular activation, thus promoting chemical bond breaking and chemical reaction. It is well known that the temperature of a metal surface increases when the metal is exposed to light for a longer period of time. Figure 2(C) shows the SERS of the conversion of PAN catalyzed by roughed Cu foil surface under different laser radiation times, the excitation wavelength was 532 nm, 50 mW power laser beam. However, the relative ratio of the D peak to G peak of graphite remains constant by increasing the irradiation time (Fig. 2(C, D)). Hence, the long exposure time is not attractive toward enhancing the catalytic reaction rates.

From the above analysis, it is apparent the significant contribution of hot-carrier interactions in the conversion of PAN molecules to graphite layer. More

Figure 2 A Raman spectra of the conversion of PAN molecules catalyzed by rough Cu foil surface under different incident laser powers. The excitation wavelength was 532 nm and the exposure time is 15 s. B Intensity ratio distribution of the D and G peaks (I_D/I_G). C SERS of the PAN conversion catalyzed by roughed Cu foil surface under different laser radiation times. The excitation wavelength was 532 nm, and the laser beam power is 50 mW. D Intensity ratio distribution of the D and G peaks (I_D/I_G).
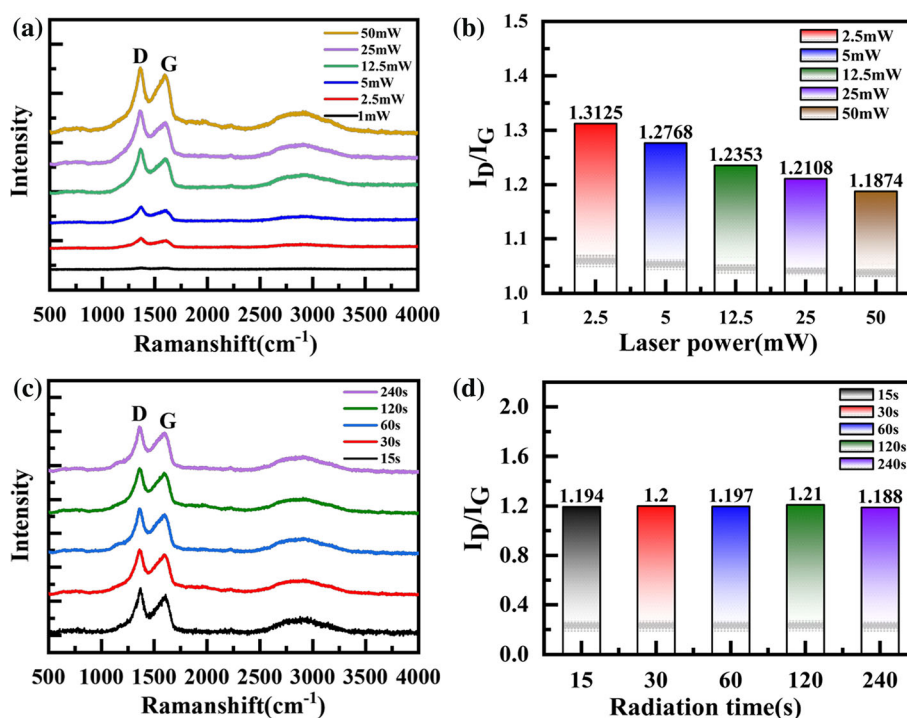
specifically, the catalytic graphitization procedures of PAN molecules are mainly influenced by the generation and migration of plasmon-induced hot carriers.

Impact of Cu nanostructure size on the catalytic graphitization process of PAN molecules

The charge density oscillations induced by the activation of plasmons as a result of the interaction of a metallic surface with light present a strong dependence from the local electric field distribution [31]. Along these lines, the modification of the surface in order to locally enhance the electric field intensity is quite crucial toward improving the efficiency of the respective plasmon-induced photocatalytic procedures. Hence, a detailed study of the influence of Cu-based nanostructures with different sizes on the catalytic graphitization processes of PAN molecules is presented below.

To ensure the necessary SERS activation, a roughening procedure was implemented on the copper substrates. Figure 3(A–C) depicts the respective AFM images of the Cu-based nanostructures revealing their morphology, whereas the histogram on the right displays their size distribution. The histogram indicated nearly normal distribution, and it is shown that the average size of copper nanostructures is about 25, 40, and 80 nm, respectively. The nanostructure size of Cu without roughening is about 10 nm. Figure 3(D) discloses the Raman spectra of catalytic graphitization process of the adsorbed PAN molecules on the surface of Cu-based nanostructures with different sizes under laser irradiation with 50 mW power. From these results, it is apparent that the relative ratio of the D to G peak acquires the smallest values when the size of the Cu-based nanostructures is 40 nm (Fig. 3e), indicating the existence of fewer defects that lead to a higher degree of graphitization. However, we have to underline that the I_D/I_G ratio is larger when the size of the Cu-based nanostructure is either 80 nm or 25 nm or the surface roughness is quite small. In addition, by calculating the defect density of graphite, we estimated the photoconversion efficiency of copper nanostructures with different sizes (Table 1). The defect density (n_D) of graphite can be calculated by the following expression [32]:

$$n_D \, (\text{cm}^{-2}) = (7.3 \pm 2.2) \times 10^9 E_L^4 \frac{I_D}{I_G}$$

As can be confirmed from Table 1, nanostructures with various sizes exhibit different photochemical conversion capabilities by retaining the laser power constant at 50 mW. Moreover, we can observe that photochemical conversion occurs more efficiently when PAN molecules are adsorbed on the surface of Cu-based nanostructures with a size of 40 nm. Under these conditions, the PAN converted to graphite with low defect density and lower relative intensity ratio of I_D/I_G. We believe this can mainly be attributed to the nanostructures of appropriate size and enhance the interaction between light and free electrons on metal surfaces, which changes the distribution of the local electromagnetic field on the surface of the nanostructure. Alternatively, the SPR properties of plasma nanomaterials are strongly dependent on the size of the formed metal nanoparticles. Thus, unique opportunities arise toward tuning the SPR frequency ($\lambda_{\max}$) to the desired value by manipulating the size of the metallic nanoparticles, resulting in the enhanced intensity of LSPR absorption peaks and electric field.

Similarly, as shown in Fig. 4(A), the ratio of the relative intensity of D and G peaks. (I_D/I_G) can be used to measure the degree of disorder, and we can see that the highest degree of catalytic graphitization of polyacrylonitrile at different solvent volatilization temperatures is achieved at a copper nanostructure size of 40 nm. Organic solvents (DMF) are difficult to evaporate completely when the temperature is below 120 °C, resulting in less graphitization of the polyacrylonitrile. Although solvents can more easily evaporate at higher temperatures, Cu-based nanostructures are susceptible to oxidation, which deteriorates the interaction between light and metal. X-ray photoelectron spectroscopy (XPS) data further supported this result. As shown in Fig. 4B, two peaks were resolved at 932.1 and 951.9 eV, which could be assigned to Cu^0 peaks [33]. Moreover, we observed two peaks at 933.9 and 953.7 eV, as well as satellite peaks near 941, 943, and 962 eV, all of which can be assigned to Cu^{II} 2p peaks [34]. As a result, the LSPR-induced generation of hot carriers will be drastically reduced, leading to a big reduction of the photochemical conversion efficiency of reactants (PAN) adsorbed on nanostructured surfaces. In order to further examine the impact of Cu oxidation, we applied the FDTD approach to calculate the local electric field strength $(E/E_0)^2$ distribution. The results
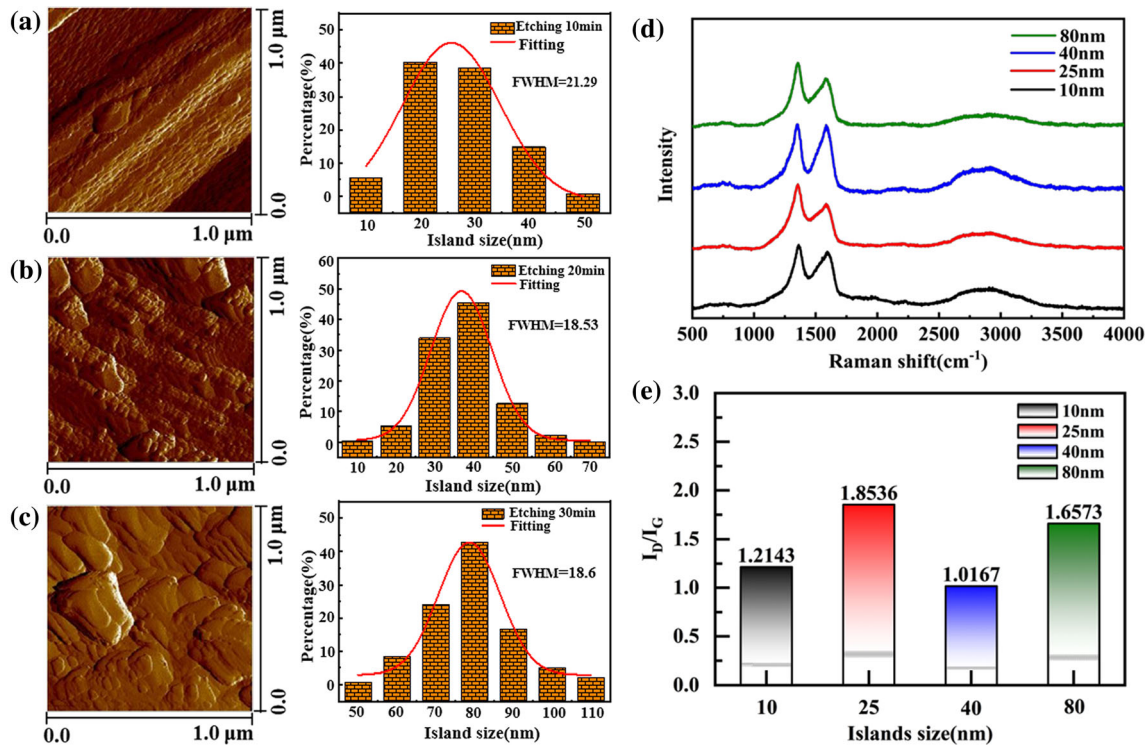
Figure 3 **A–C** AFM images of Cu-based nanostructures with different sizes (left) and the respective histograms revealing their size distributions (Right). **D** Raman spectra of the catalytic graphitization process of PAN molecules on Cu nanostructures with different sizes. **E** Distribution of the I_D/I_G ratios for the conversion of PAN molecules to graphite on Cu-based nanostructures with various sizes.

Table 1 Defect density and I_D/I_G of the graphite

Size	10 nm	25 nm	40 nm	80 nm
I_D/I_G	1.8595	2.1350	1.0467	1.6573
n_D (cm^{-2}) × 10^7	17.67	20.28	9.95	15.74

indicate a significant decrease of the local electric field intensity when an oxide layer has been formed on the surface of copper. According to previously reported theoretical and experimental studies, the rate of carrier generation from plasmon decay procedures is directly proportional to the local electric field intensity [35, 36]. Therefore, an enhanced electric field distribution within the Cu-based nanostructures decisively impacts the hot-carrier formation rate induced by non-radiative plasmon decay processes. Along these lines, the formation of a Cu oxide layer contributes destructively to the catalytic graphitization properties of PAN molecules.

Simulating the local electric field distribution and the mechanism of the hot-carrier-driven catalysis

From the abovementioned experimental data, we can draw the conclusion that the optimum conditions for an enhanced catalytic graphitization degree of the PAN molecules are achieved by tuning the size of the respective Cu-based nanostructures. The local electric field distribution on the surface of a nanostructure can be adjusted by modulating the size of the formed metal nanoparticles, thus improving the chemical conversion efficiency. To further confirm our conclusions, the FDTD method was applied to calculate the local electric field patterns induced from different nanostructure sizes. The choice of model structure depended mainly on the AFM image of the copper nanostructure. All AFM images were inputted to an FDTD software to obtain Model 1, Model 2 and Model 3. The results (Fig. 5A–C) divulge the development of quite high local electric field values whereas the displayed color scale bars represent the respective electric field enhancement ($|E|/|E_0|$)^2
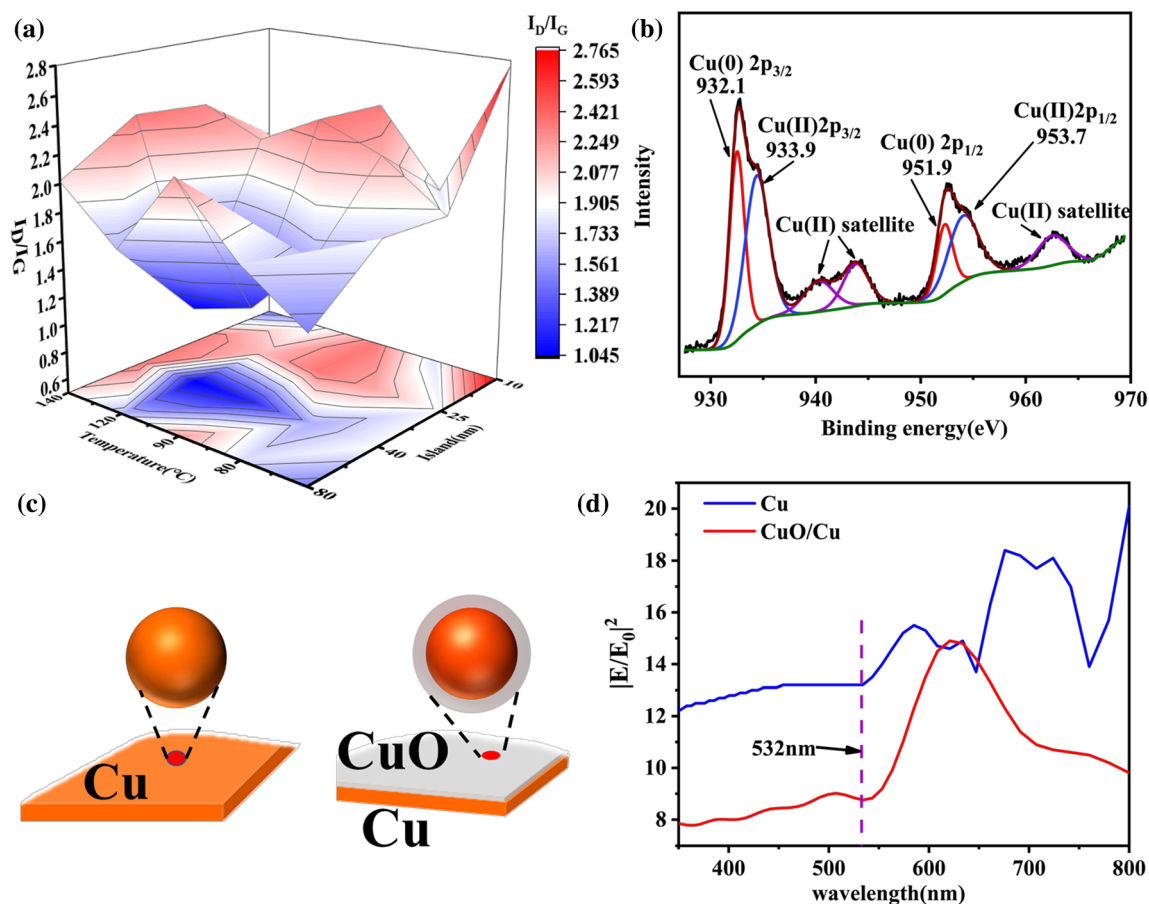
Figure 4 **A** Distribution of intensity ratio between D and G peaks (I_D/I_G) of PAN-catalyzed graphite by employing different solvent volatilization temperatures and different Cu sizes. **B** X-ray photoelectron spectroscopy (XPS) of Cu surfaces. **C** Schematic diagram of Cu and Cu/CuO. **D** Calculated local electric field strength $|E/E_0|^2$ in Cu and CuO/Cu through a FDTD model.

values obtained in each case. These areas are also called "hot spots" since the intensity of the local electric field within these areas increases by several orders of magnitude.

Moreover, as can be ascertained from Fig. 5A–C, the biggest values of the local electric field are obtained by using nanoparticles with size of 40 nm (Model 2), while the two other configurations(Model 1, Model 3) of the metallic surface (25 and 80 nm) produced smaller enhancements. This effect is in direct line with the respective experimental data, where the highest degree of graphitization of PAN molecules was obtained by using an average size for the Cu-based nanostructures of 40 nm, denoting the validity of our theoretical framework. Meanwhile, we obtained the extinction spectra of three different nanostructures by FDTD calculation (see Supplementary Information Figure S7). The extinction phenomenon in SPR is composed of absorption and

scattering, and a local surface-enhanced electric field is generated on the metal surface. Compared with model 1 and model 3, model 2 can obtain the value of larger extinction cross section. Therefore, the very high extinction cross section will cause a huge enhancement of the electric field strength.

In addition, the electric field intensity exhibits a strong dependence on the size of the plasmonic nanostructures, since a quite small nanocrystal size leads to an SPR effect with a short lifetime. This effect is nicely captured by the following equation, where the rate of plasmon-induced hot-carrier generation can be estimated [30]

$$P_{MFP} = \frac{1}{2} \int_{V_{MFP}} d\mathbf{r} |E(r)|^2 \mathrm{Im}(\varepsilon)$$

where $|E(r)|^2$ is the local electric field intensity, $\mathrm{Im}(\varepsilon)$ is the imaginary part of the material's dielectric function, P_{MFP} is the optical absorption within the

Figure 5 A–C The FDTD simulated results and the near-field electric field distribution. Different sizes of Cu nanoparticles were taken into consideration.
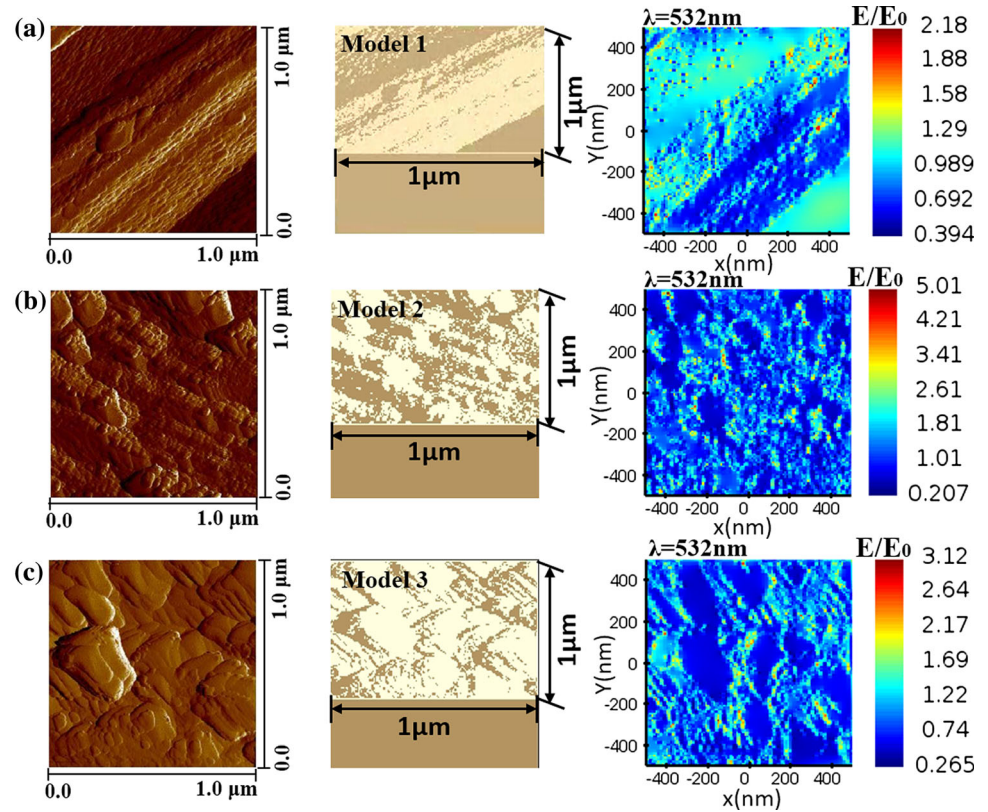
mean free path length of the transmission interface, and V_{MFP} is the under consideration metallic volume that includes the mean free path of the transmission interface. Thus, we can conclude that the excitation rate of hot carriers due to the implementation of the SPR effect on plasmonic nanostructures exhibits a strong dependence on local electric field distribution while the intensity of this effect can be modulated by controlling the size of the particles. Additionally, the resonance frequency coupling between the photons and the plasmons is strongly correlated with the local electric field distribution at the surface of the nanoparticles. An enhanced electric field can lead to the creation of a bigger number of energetic charge carriers (electron–hole pairs). The hot carriers in the metal structure are subsequently injected into the available orbitals of the adjacent PAN molecules, which can promote the chemical transformation procedures.

Conclusions

In this work, we investigated the catalytic graphitization processes of PAN molecules on the surface of roughed Cu foils by employing in situ SERS. From our experimental results, it is apparent that the PAN molecules are adsorbed on the surface of Cu foil, which was subsequently transformed into a graphite layer under laser beam irradiation at 532 nm. According to our experiment and theoretical model, the catalytic graphitization procedures of PAN molecules are triggered by the generation of hot carriers in the Cu-based nanoparticles. Moreover, the size of Cu-based nanostructures plays also a key role in enhancing the low-temperature catalytic graphitization performance of PAN molecules. The outcome of our simulation by using the FDTD method indicates that the local electric field distribution presents a strong dependence on the size of the Cu-based nanostructures. The experimental results are in direct line with the assumption that the excitation on plasmonic nanostructures results in increased generation rates of hot carriers due to the local electric field enhancement.

Acknowledgements

Author contributions

ZZ performed the experiment, data analyses and wrote the manuscript; HT, JL, and XR contributed significantly to analysis and manuscript preparation; NS, JL, YG, YZ, XC, and JC helped perform the analysis with constructive discussions.

Declarations

Conflict of interest The authors declare that they have no known competing financial interests or personal relationships that could have appeared to influence the work reported in this paper.

Supplementary Information: The online version contains supplementary material available at https://doi.org/10.1007/s10853-021-06742-z.

References

[1] Lu J, Li W, Kang H et al (2020) Microstructure and properties of polyacrylonitrile based carbon fibers. Polym Test 81:106267. https://doi.org/10.1016/j.polymertesting.2019.106267

[2] Barton BE, Behr MJ, Patton JT et al (2017) High-modulus low-cost carbon fibers from polyethylene enabled by boron catalyzed graphitization. Small 13:1701926. https://doi.org/10.1002/smll.201701926

[3] Chen L, Fang T, Song C et al (2021) Catalytic graphitization of boron on the fabrication of high-performance carbon papers for gas diffusion layers in PEMFCs. Catal Commun 157:106332. https://doi.org/10.1016/j.catcom.2021.106332

[4] He D, Zhang F, Xu S et al (2008) Synergistic catalytic effect of Ti–B on the graphitization of polyacrylonitrile-based carbon fibers. Carbon 46:1506–1508. https://doi.org/10.1016/j.carbon.2008.06.043

[5] Zhang H, Wei J, Zhang X-G et al (2020) Plasmon-induced interfacial hot-electron transfer directly probed by Raman spectroscopy. Chem 6:689–702. https://doi.org/10.1016/j.chempr.2019.12.015

[6] Cong S, Liu X, Jiang Y et al (2020) Surface enhanced raman scattering revealed by interfacial charge-transfer transitions. Innovation 1:100051. https://doi.org/10.1016/j.xinn.2020.100051

[7] Zhao LB, Zhang M, Huang YF et al (2014) Theoretical study of plasmon-enhanced surface catalytic coupling reactions of aromatic amines and nitro compounds. J Phys Chem Lett 5:1259. https://doi.org/10.1021/jz5003346

[8] Bhattacharya C, Saji SE, Mohan A et al (2020) Sustainable nanoplasmon-enhanced photoredox reactions: synthesis, characterization, and applications. Adv Energy Mater 10:2002402. https://doi.org/10.1002/aenm.202002402

[9] Linic S, Aslam U, Boerigter C et al (2015) Photochemical transformations on plasmonic metal nanoparticles. Nat Mater 14:567–576. https://doi.org/10.1038/nmat4281

[10] Zhang Z, Xu P, Yang X et al (2016) Surface plasmon-driven photocatalysis in ambient, aqueous and high-vacuum monitored by SERS and TERS. J Photochem Photobiol C Photochem Rev 27:100–112. https://doi.org/10.1016/j.jphotochemrev.2016.04.001

[11] Kazuma E, Kim Y (2019) Mechanistic studies of plasmon chemistry on metal catalysts. Angew Chem Int Ed Engl 58:4800–4808. https://doi.org/10.1002/anie.201811234

[12] Huang C, Jevric M, Borges A et al (2017) Single-molecule detection of dihydroazulene photo-thermal reaction using break junction technique. Nat Commun 8:15436. https://doi.org/10.1038/ncomms15436

[13] Robatjazi H, Zhao H, Swearer DF et al (2017) Plasmon-induced selective carbon dioxide conversion on earth-abundant aluminum-cuprous oxide antenna-reactor nanoparticles. Nat Commun 8:27. https://doi.org/10.1038/s41467-017-00055-z

[14] Wu K, Chen J, McBride JR (2015) Efficient hot-electron transfer by a plasmon-induced interfacial charge-transfer transition. Science 349:632–635. https://doi.org/10.1126/science.aac5443

[15] Adriana IH, Alejandro VR, Velia O (2018) Synthesis of graphite oxide with different surface oxygen contents assisted microwave radiation. Nanomaterials 8:1–17. https://doi.org/10.3390/nano8020106

[16] Liu Z, Hou W, Pavaskar P et al (2011) Plasmon resonant enhancement of photocatalytic water splitting under visible illumination. Nano Lett 11:1111–1116. https://doi.org/10.1021/nl104005n

[17] Sun M, Xu H (2012) A novel application of plasmonics: plasmon-driven surface-catalyzed reactions. Small 8:2777–2786. https://doi.org/10.1002/smll.201200572

[18] Zhang P, Liu H, Li X (2021) Photo-reduction synthesis of Cu nanoparticles as plasmon-driven non-semiconductor

photocatalyst for overall water splitting. Appl Surf Sci 535:147720. https://doi.org/10.1016/j.apsusc.2020.147720

[19] Hu C, Chen X, Jin J et al (2019) Surface plasmon enabling nitrogen fixation in pure water through a dissociative mechanism under mild conditions. J Am Chem Soc 141:7807–7814. https://doi.org/10.1021/jacs.9b01375

[20] Yao GY, Zhao ZY, Liu QL et al (2020) Theoretical calculations for localized surface plasmon resonance effects of Cu/TiO_2 nanosphere: generation, modulation, and application in photocatalysis. Sol Energy Mater Sol Cells 208:110385. https://doi.org/10.1016/j.solmat.2019.110385

[21] Gawande MB, Goswami A, Felpin FX et al (2016) Cu and Cu-based nanoparticles: synthesis and applications in catalysis. Chem Rev 116:3722–3811. https://doi.org/10.1021/acs.chemrev.5b00482

[22] Babar S, Weaver JH (2015) Optical constants of Cu, Ag, and Au revisited. Appl Opt 54:477. https://doi.org/10.1364/ao.54.000477

[23] Brimhall N, Herrick N, Allred DD et al (2010) Measured optical constants of copper from 10 nm to 35 nm. Opt Express 17:23873–23879. https://doi.org/10.1364/OE.17.023873

[24] Xu K, Zhou R, Takei K et al (2019) Toward flexible Surface-Enhanced Raman Scattering (SERS) sensors for point-of-care diagnostics. Adv Sci 6:1900925. https://doi.org/10.1002/advs.201900925

[25] Schranghamer TF, Oberoi A, Das S (2020) Graphene memristive synapses for high precision neuromorphic computing. Nat Commun 11:5474. https://doi.org/10.1038/s41467-020-19203-z

[26] Shao X, Srinivasan A, Ang WK et al (2018) A high-brightness large-diameter graphene coated point cathode field emission electron source. Nat Commun 9:1288. https://doi.org/10.1038/s41467-018-03721-y

[27] Nidhankar AD, Goudappagouda WVC et al (2021) Efficient metal-free organic room temperature phosphors. Chem Sci 12:4216–4236. https://doi.org/10.1039/d1sc00446h

[28] Sakamoto M, Kawawaki T, Kimura M et al (2019) Clear and transparent nanocrystals for infrared-responsive carrier transfer. Nat Commun 10:406. https://doi.org/10.1038/s41467-018-08226-2

[29] Christopher P, Xin H, Linic S (2011) Visible-light-enhanced catalytic oxidation reactions on plasmonic silver nanostructures. Nat Chem 3:467–472. https://doi.org/10.1038/nchem.1032

[30] Christopher P, Moskovits M (2017) Hot charge carrier transmission from plasmonic nanostructures. Annu Rev Phys Chem 68:379–398. https://doi.org/10.1146/annurev-physchem-052516-044948

[31] Zhang Z, Zhang C, Zheng H et al (2019) Plasmon-driven catalysis on molecules and nanomaterials. Acc Chem Res 52:2506–2515. https://doi.org/10.1021/acs.accounts.9b00224

[32] Li B, Zhou L, Wu D et al (2011) Photochemical chlorination of graphene. ACS Nano 5:5957–5961. https://doi.org/10.1021/nn201731t

[33] Jiang Z, Sun W, Miao W et al (2019) Living atomically dispersed Cu ultrathin TiO_2 nanosheet CO_2 reduction photocatalyst. Adv Sci 6:1900289. https://doi.org/10.1002/advs.201900289

[34] Lyu Z, Xie M, Aldama E et al (2019) Au@Cu core-shell nanocubes with controllable sizes in the range of 20–30 nm for applications in catalysis and plasmonics. ACS Appl Nano Mater 2:1533–1540. https://doi.org/10.1021/acsanm.9b00016

[35] Manjavacas A, Liu JG, Kulkarni V et al (2014) Plasmon-induced hot carriers in metallic nanoparticles. ACS Nano 8:7630–7638. https://doi.org/10.1021/nn502445f

[36] Zheng BY, Zhao H, Manjavacas A et al (2015) Distinguishing between plasmon-induced and photoexcited carriers in a device geometry. Nat Commun 6:7797. https://doi.org/10.1038/ncomms8797